Pedestrian Intensive Scanning for Active-scan LIDAR

Taiki Yamamoto[1], Fumito Shinmura[2], Daisuke Deguchi[3],
Yasutomo Kawanishi[1], Ichiro Ide[1] and Hiroshi Murase[1]
[1]*Graduate School of Informatics, Nagoya University, Furo-cho, Chikusa-ku, Nagoya-shi, Aichi, Japan*
[2]*Institutes of Innovation for Future Society, Nagoya University, Furo-cho, Chikusa-ku, Nagoya-shi, Aichi, Japan*
[3]*Information Strategy Office, Nagoya University, Furo-cho, Chikusa-ku, Nagoya-shi, Aichi, Japan*

Keywords: Active-scan LIDAR, Stochastic Sampling, Pedestrian Detection.

Abstract: In recent years, LIDAR is playing an important role as a sensor for understanding environments of a vehicle's surroundings. Active-scan LIDAR is being actively developed as a LIDAR that can control the laser irradiation direction arbitrary and rapidly. In comparison with conventional uniform-scan LIDAR (e.g. Velodyne HDL-64e), Active-scan LIDAR enables us to densely scan even distant pedestrians. In addition, if appropriately controlled, this sensor has a potential to reduce unnecessary laser irradiations towards non-target objects. Although there are some preliminary studies on pedestrian scanning strategy for Active-scan LIDARs, in the best of our knowledge, an efficient method has not been realized yet. Therefore, this paper proposes a novel pedestrian scanning method based on orientation aware pedestrian likelihood estimation using the orientation-wise pedestrian's shape models with local distribution of measured points. To evaluate the effectiveness of the proposed method, we conducted experiments by simulating Active-scan LIDAR using point-clouds from the KITTI dataset. Experimental results showed that the proposed method outperforms the conventional methods.

1 INTRODUCTION

In recent years, development of autonomous driving systems and Advanced Driver Assistance Systems (ADAS) is attracting attention all over the world. Collision avoidance is one of the most important function in these systems to reduce traffic accidents, and recognition of surrounding environments is indispensable for developing these systems. Currently, various types of sensors have been developed and some of them are commercially available. Among them, LIDAR (LIght Detection And Ranging) is now widely implemented as an in-vehicle sensor for recognizing the surrounding environment. LIDAR can simultaneously measure the distance to target objects and their reflection intensities by irradiating laser rays and measuring their reflections. Velodyne LiDAR[1] is one of the most popular LIDAR in recent years, which is equipped with multiple laser irradiation ports in the vertical direction as shown in Fig. 1. Irradiating laser rays by rotating the sensor itself in the horizontal direction, it can obtain a point-cloud of 360 degrees view uniformly (We call this type of LIDAR as "uniform-scan LIDAR"). In addition, according to the increase of laser irradiation ports, the vertical density of the point-cloud can be increased.

Some research groups tackled the problem of pedestrian detection devising uniform-scan LIDARs (Kidono et al., 2011; Behley et al., 2013; Maturana and Scherer, 2015; Wang et al., 2017; Tatebe et al., 2018; Zhou and Oncel, 2018). Kidono et al. proposed two kinds of features for recognizing pedestrians using a dense uniform-scan LIDAR (Kidono et al., 2011). Their method extracts a slice feature which is defined by the horizontal and depth sizes of 3D point-clouds in each vertically sliced section for a rough shape representation. In addition, they proposed an additional feature which is the reflection intensity distribution for representing the material of the target surface. Based on these features, it is possible to distinguish pedestrians with non-pedestrians such as poles. Although their method succeeded to detect most pedestrians, its accuracy degraded if the target pedestrian exists in a distant position.

To cope with this problem, Tatebe et al. proposed a voxel representation method applicable to sparse point-clouds that are obtained from distant targets (Tatebe et al., 2018). Their method combined

[1]Velodyne LiDAR, Inc. https://velodynelidar.com/

Yamamoto, T., Shinmura, F., Deguchi, D., Kawanishi, Y., Ide, I. and Murase, H.
Pedestrian Intensive Scanning for Active-scan LIDAR.
DOI: 10.5220/0007359903130320
In *Proceedings of the 14th International Joint Conference on Computer Vision, Imaging and Computer Graphics Theory and Applications (VISIGRAPP 2019)*, pages 313-320
ISBN: 978-989-758-354-4
Copyright © 2019 by SCITEPRESS – Science and Technology Publications, Lda. All rights reserved

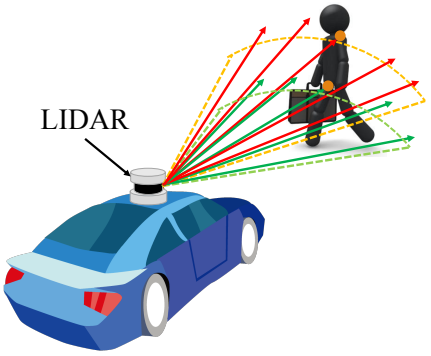

Figure 1: Scanning using a LIDAR.

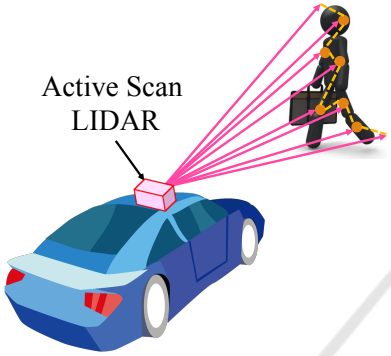

Figure 2: Scanning using an Active Scan LIDAR.

the voxel representation and 3DCNN for pedestrian detection. By using the characteristic that the beam width of an irradiated laser ray increases according to the distance from the sensor, their method estimates the distribution of the target point-cloud and uses it for constructing a voxel representation. Although they succeeded to detect distant pedestrians, their method still failed if the density of the target point-cloud is extremely low. Therefore, improvement of the point-cloud density will be the key factor to improve the detection accuracy of distant pedestrians. However, it is difficult for an uniform-scan LIDAR to increase the vertical density of the point-cloud because the number of laser irradiation ports is limited.

Recently, some manufacturers are trying to develop new types of LIDARs that can control the laser irradiation direction arbitrary and rapidly as shown in Fig. 2, such as Blackmore Sensors and Analytics, Inc[2]. Hereafter, we call these types of sensors as Active-scan LIDAR. It has a great advantage which enables us to scan arbitral 3D positions quickly and programmatically. If we can control it appropriately, we can expect to obtain a dense point-cloud of distant pedestrians as same as close pedestrians. Since scanning time increases according to the number of irradiated laser rays, it is necessary to properly set laser irradiation directions to obtain a dense point-cloud of pedestrians efficiently.

To solve this problem, we proposed a progressive scan strategy using pedestrian's shape model to obtain dense point-clouds from pedestrians (Yamamoto et al., 2018). Although the observable pedestrian's shape changes according to the viewpoint (or pedestrian's orientation), the method did not consider the variations of observable shapes. In addition, since the method constructed a pedestrian likelihood map by assuming that all measured points came from pedestrians, we did not segregate the measured points from non-pedestrian objects. Thus, it was difficult to distinguish a point-cloud of a pedestrian from that of a non-pedestrian object, such as a pole or a tree that has a similar shape as a pedestrian but has a different size.

To overcome the above problems, this paper proposes an orientation-aware pedestrian scanning method that enables us to scan pedestrians densely with a small number of laser irradiations. In the proposed method, the pedestrian's orientation is considered when constructing his/her shape model. Moreover, a pedestrian likelihood map is calculated by considering whether the measured points came from the same object or not. Here, depth-wise object separation is used. Finally, we formulate the selection of laser irradiation directions as a problem in a stochastic sampling framework based on the pedestrian likelihood map.

The contributions of this paper are as follows:

1. Estimation of a pedestrian likelihood map considering observable pedestrian's shape variation according to his/her orientation.
2. Introduction of depth-wise object separation for constructing the pedestrian likelihood map considering whether the measured points came from the same object or not.

2 IDEAS FOR EFFICIENT SCANNING

This section describes the basic ideas to efficiently obtain a dense point-cloud from a pedestrian efficiently devising an Active-scan LIDAR. In order to select appropriate laser irradiation directions, the proposed method employs a stochastic sampling framework based on a pedestrian likelihood map representing the existence of pedestrians. Here, the primary pedestrian likelihood map is constructed by the initial

[2]Blackmore Sensors and Analytics, Inc. https://blackmoreinc.com/

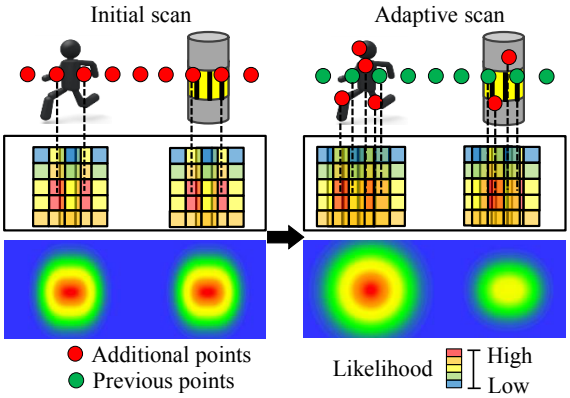

Figure 3: Increasing the number of measured points and updating the pedestrian likelihood map by adaptive scan.

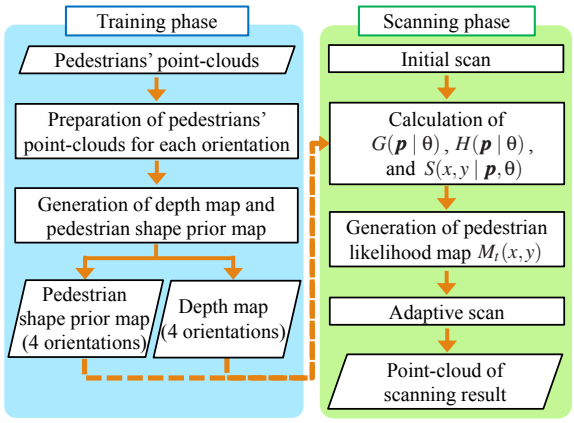

Figure 4: Process-flow of the proposed method.

scan, and then the proposed method progressively updates the pedestrian likelihood map based on the measured points by additional laser irradiations where their directions are set adaptively. By repeating this step, the pedestrian likelihood map gradually improves even if the initial point-cloud is sparse, as shown in Fig. 3.

Here, considering the observable shape variations among front, back, right, and left orientations, multiple pedestrian's shape models are integrated to compute the pedestrian likelihood map. Futhermore, the pedestrian likelihood map is calculated by considering whether the measured points came from the same object or not. Here, depth-wise object separation based on the pedestrian's shape model is applied to judge whether the points are measured within the same object or not. Then, the proposed method calculates the ratio of pedestrian/non-pedestrian points based on the above, and uses it for controlling the weights representing the goodness of fitted pedestrian's shape model. Finally, the selection of the next laser irradiation directions are stochastically sampled from the pedestrian likelihood map.

Here, the pedestrian likelihood map $M_t(x,y)$ in the t-th iteration is calculated as

$$M_t(x,y) = \sum_{\boldsymbol{p}\in\mathcal{P}_t} \sum_{\theta} F(x,y \mid \boldsymbol{p},\theta), \qquad (1)$$

where $\mathcal{P}_t$ is a point-cloud obtained until the t-th scan, θ is a parameter corresponding to the orientation of the pedestrian's model, and $F(x,y \mid \boldsymbol{p},\theta)$ is a local pedestrian likelihood map when a point $\boldsymbol{p}$ and θ are given. The local pedestrian likelihood map $F(x,y \mid \boldsymbol{p},\theta)$ is calculated as

$$F(x,y \mid \boldsymbol{p},\theta) = G(\boldsymbol{p} \mid \theta) H(\boldsymbol{p} \mid \theta) S(x,y \mid \boldsymbol{p},\theta), \qquad (2)$$

where $G(\boldsymbol{p} \mid \theta)$ represents the goodness of the fitted pedestrian's shape model around the given $\boldsymbol{p}$, $H(\boldsymbol{p} \mid \theta)$ represents the degree of object isolation around $\boldsymbol{p}$, and $S(x,y \mid \boldsymbol{p},\theta)$ is the local probability map representing pedestrian existence around $\boldsymbol{p}$.

Based on the stochastic sampling from the pedestrian likelihood map $M_t(x,y)$, the directions of the laser irradiations for the $(t+1)$-th scan are calculated. After completing the $(t+1)$-th scan, the $(t+1)$-th pedestrian likelihood map $M_{t+1}(x,y)$ is calculated.

3 ADAPTIVE SCANNING BASED ON PEDESTRIAN LIKELIHOOD

This section describes the proposed method to realize the ideas explained in Section 2. Figure 4 shows the process-flow of the proposed method. It consists of the following two phases:

1. Training phase
   (a) Preparation of pedestrians' point-clouds for each orientation
   (b) Generation of depth maps and pedestrian shape prior maps
2. Scanning phase
   (a) Initial scan
   (b) Calculation of $G(\boldsymbol{p} \mid \theta)$, $H(\boldsymbol{p} \mid \theta)$, and $S(x,y \mid \boldsymbol{p},\theta)$ using depth maps and pedestrian shape prior maps
   (c) Calculation of pedestrian likelihood map $M_t(x,y)$
   (d) Adaptive scan based on pedestrian likelihood map $M_t(x,y)$
   (e) Repeat 2(b) to 2(e)

In the training phase, depth maps and pedestrian shape prior maps are constructed from manually ex-

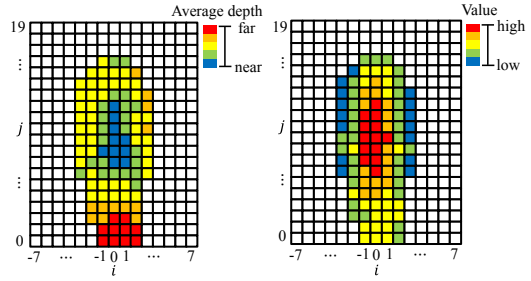

(a) Depth map. (b) Pedestrian shape prior map.

Figure 5: Example of a depth map and a pedestrian shape prior map for the front orientation.

tracted pedestrians' point-clouds, and their orientations are also manually annotated. In the scanning phase, laser irradiation directions are adaptively selected based on a stochastic sampling from the pedestrian likelihood map $M_t(x,y)$, and those measurement results are used for updating the pedestrian likelihood map $M_{t+1}(x,y)$ for the next scan. Details of each process are described below.

3.1 Training Phase

This section describes the generation of two maps that represent depth and pedestrian shape prior for each orientation of pedestrians. The depth maps are used for calculating $G(\boldsymbol{p} \mid \theta)$ and $H(\boldsymbol{p} \mid \theta)$ and the pedestrian shape prior maps are used to calculate $S(x,y \mid \boldsymbol{p},\theta)$ in Eq. (2). In the following explanation, for simplicity, the position of LIDAR is set at the origin of the coordinate system, and x-, y-, and z-axes of the coordinate system correspond to the lateral, the vertical, and the depth directions of the vehicle, respectively.

3.1.1 Preparation of Pedestrians' Point-clouds for Each Orientation

First of all, pedestrians' point-clouds are extracted from LIDAR data, and then they are classified into four pedestrian's orientation (front, back, left, right) manually. Here, pedestrians' point-clouds difficult to be classified into any of the four orientations are discarded.

3.1.2 Calculation of Depth Maps and Pedestrian Shape Prior Maps

The depth maps and the pedestrian shape priors are calculated by integrating pedestrians' point-clouds in each orientation. Figure 5 shows an example of a depth map and a pedestrian shape prior map for the front orientation.

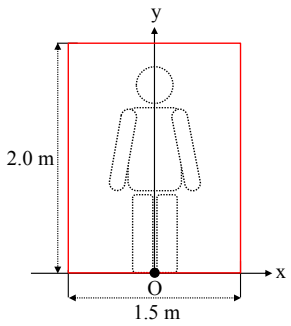

Figure 6: Points are extracted from an area with a size of 1.5 m $\times$ 2.0 m.

The first step is the integration of pedestrians' point-clouds in each orientation. Here, point-clouds are aligned by shifting each point-cloud so that the smallest vertical coordinate (y-axis), depth coordinate (z-axis), and the average of the lateral coordinate (x-axis) become zero. After the alignment, as shown in Fig. 6, points are extracted from an area with a size of 1.5 m $\times$ 2.0 m. Finally, the integrated point-clouds are divided into 15×20 cells and are used for calculating the depth map and the pedestrian shape prior map. Here, each cell has a size of $W \times W$ ($W = 0.1$ m), and is identified using horizontal and vertical indices ($i = -7,-6,\ldots,0,\ldots,6,7$, $j = 0,1,\ldots,19$).

From the integrated point-clouds, the depth map of each orientation $d(i,j \mid \theta)$ is calculated as the average depth in each cell where θ is a parameter indicating the orientation of the pedestrian's model. Also, the pedestrian shape prior map of each orientation $s(i,j \mid \theta)$ is calculated based on the number of points $n(i,j \mid \theta)$ contained in each cell as

$$s(i,j \mid \theta) = \begin{cases} \dfrac{n(i,j \mid \theta)}{\sum_{k,\ell} n(k,\ell \mid \theta)} & \text{if } n(i,j \mid \theta) \geq 10 \\ & \text{and } |i| \leq 7 \\ & \text{and } 0 \leq j \leq 19 \\ 0 & \text{otherwise} \end{cases} \tag{3}$$

Here, to reduce the effect of noise, if the cell satisfies $n(i,j \mid \theta) < 10$, they are treated as $d(i,j \mid \theta) = \infty$ and $n(i,j \mid \theta) = 0$. Finally, $d(i,j \mid \theta)$ and $s(i,j \mid \theta)$ are used as a depth map and a pedestrian shape prior map, respectively.

3.2 Scanning Phase

This section describes the adaptive selection of laser irradiation directions based on a stochastic sampling from the pedestrian likelihood map. Details on the calculation process of the pedestrian likelihood map is also described.

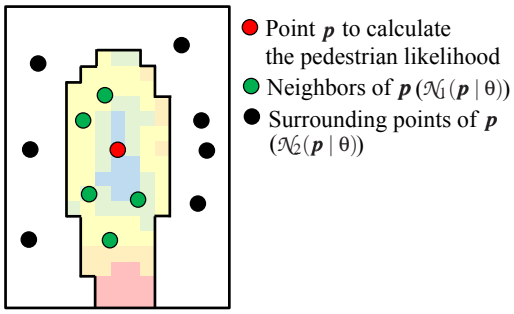

Figure 7: Points used for calculating the weights $G(\boldsymbol{p} \mid \theta)$ and $H(\boldsymbol{p} \mid \theta)$.

3.2.1 Initial Scan

As the first step, the initial scan is performed to find a pedestrian by a small number of laser irradiations to obtain the rough shape and position of each object in a scene. Here, the initial number of laser irradiations is N_0, and each laser ray is irradiated at a certain interval along the horizontal direction at a constant height h. After the initial scan, a horizontally dense point-cloud at the height h is obtained.

3.2.2 Calculation of Weights and the Local Probability Map using Depth Maps and Pedestrian Shape Prior Maps

As the second step, the global pedestrian likelihood map (Eq. (2)) is calculated by $G(\boldsymbol{p} \mid \theta)$, $H(\boldsymbol{p} \mid \theta)$, and $S(x,y \mid \boldsymbol{p},\theta)$ where $S(x,y \mid \boldsymbol{p},\theta)$ is the local probability map around $\boldsymbol{p}$, and $G(\boldsymbol{p} \mid \theta)$ and $H(\boldsymbol{p} \mid \theta)$ are weights for controlling the integration of $S(x,y \mid \boldsymbol{p},\theta)$.

First of all, based on a point $\boldsymbol{p} \in \mathcal{P}_t$ obtained after the t-th scan, $G(\boldsymbol{p} \mid \theta)$ representing the goodness of the fitted pedestrian's shape is calculated as

$$G(\boldsymbol{p} \mid \theta) = \frac{1}{|\mathcal{N}_1(\boldsymbol{p} \mid \theta)|} \sum_{\boldsymbol{q} \in \mathcal{N}_1(\boldsymbol{p} \mid \theta)} \phi(\boldsymbol{p},\boldsymbol{q} \mid \theta), \quad (4)$$

where $\mathcal{N}_1(\boldsymbol{p} \mid \theta)$ is a set of neighbor points coming from the same object around $\boldsymbol{p}$ and $|\mathcal{N}_1(\boldsymbol{p} \mid \theta)|$ is the number of points in $\mathcal{N}_1(\boldsymbol{p} \mid \theta)$. $\mathcal{N}_1(\boldsymbol{p} \mid \theta)$ is obtained as

$$\begin{aligned}\mathcal{N}_1(\boldsymbol{p} \mid \theta) = \{\boldsymbol{q} \mid \boldsymbol{q} \in \mathcal{P}_t, \phi(\boldsymbol{p},\boldsymbol{q} \mid \theta) \neq 0,\\ |q_x - p_x| \leq 0.75 \text{ m}, 0 \text{ m} \leq q_y \leq 2 \text{ m},\\ |q_z - p_z| \leq 1 \text{ m}\},\end{aligned} \quad (5)$$

where $\boldsymbol{p} = (p_x, p_y, p_z)$ and $\boldsymbol{q} = (q_x, q_y, q_z)$. An example of neighbor points of a pedestrian around $\boldsymbol{p}$ (red point) is shown in Fig. 7 (green points). Here, $\phi(\boldsymbol{p},\boldsymbol{q} \mid \theta)$ is a normal distribution whose average and variance are $\mu = d(i,j \mid \theta) - d(0,c \mid \theta)$ and σ^2, respectively, and is calculated as

$$\phi(\boldsymbol{p},\boldsymbol{q} \mid \theta) = \begin{cases} \exp\left(-\frac{((q_z - p_z) - \mu)^2}{2\sigma^2}\right) & \text{if } d(i,j \mid \theta) \neq \infty \\ 0 & \text{otherwise} \end{cases}, \quad (6)$$

where $d(0,c \mid \theta)$ is the depth of the cell $(0,c)$ containing $\boldsymbol{p}$, and $d(i,j \mid \theta)$ is the depth of the cell (i,j) containing $\boldsymbol{q}$. The indices i, j, and c are calculated as

$$i = \left\lfloor \frac{q_x - p_x}{W} \right\rfloor, j = \left\lfloor \frac{q_y}{W} \right\rfloor, c = \left\lfloor \frac{p_y}{W} \right\rfloor. \quad (7)$$

Note that $\lfloor \cdot \rfloor$ is a floor function defined as

$$\lfloor x \rfloor = \max\{n \mid \forall n \in \mathbb{I}, n \leq x\}, \quad (8)$$

where $\mathbb{I}$ is a set of whole integers.

$H(\boldsymbol{p} \mid \theta)$ corresponds to the weight for controlling the effect of $G(\boldsymbol{p} \mid \theta)$ based on depth-wise object separation around $\boldsymbol{p}$, which is calculated as

$$H(\boldsymbol{p} \mid \theta) = \frac{|\mathcal{N}_1(\boldsymbol{p} \mid \theta)|}{|\mathcal{N}_2(\boldsymbol{p} \mid \theta)|}, \quad (9)$$

where $\mathcal{N}_2(\boldsymbol{p} \mid \theta)$ is a set of surrounding points coming from different objects around $\boldsymbol{p}$ (black points) and $|\mathcal{N}_2(\boldsymbol{p} \mid \theta)|$ is the number of points in $\mathcal{N}_2(\boldsymbol{p} \mid \theta)$. Here, $\mathcal{N}_2(\boldsymbol{p} \mid \theta)$ is obtained as

$$\begin{aligned}\mathcal{N}_2(\boldsymbol{p} \mid \theta) = \{\boldsymbol{q} \mid \boldsymbol{q} \in \mathcal{P}_t, \phi(\boldsymbol{p},\boldsymbol{q} \mid \theta) = 0,\\ |q_x - p_x| \leq 0.75 \text{ m}, 0 \text{ m} \leq q_y \leq 2 \text{ m},\\ |q_z - p_z| \leq 1 \text{ m}\}.\end{aligned} \quad (10)$$

$S(x,y \mid \boldsymbol{p},\theta)$ is the local probability map representing the existence of a pedestrian around $\boldsymbol{p}$, which is calculated as

$$S(x,y \mid \boldsymbol{p},\theta) = s\left(\left\lfloor \frac{x - p_x}{W'} \right\rfloor, \left\lfloor \frac{y}{W'} \right\rfloor \middle| \theta\right), \quad (11)$$

where W' is calculated as

$$W' = \frac{W}{p_z}. \quad (12)$$

3.2.3 Calculation of Pedestrian Likelihood Map

As the third step, the pedestrian likelihood map $M_t(x,y)$ is generated using the weights $G(\boldsymbol{p} \mid \theta)$ and $H(\boldsymbol{p} \mid \theta)$ and the local probability map $S(x,y \mid \boldsymbol{p},\theta)$ derived in Section 3.2.2.

The pedestrian likelihood map $M_t(x,y)$ is calculated by Eqs. (1) and (2).

3.2.4 Adaptive Scan based on the Pedestrian Likelihood Map

Finally, the laser irradiation directions are selected for the next scan. The stochastic sampling referring to the probability of the existence of pedestrians represented by the pedestrian likelihood map $M_t(x,y)$ is applied to select irradiation directions. Here, the inverse transform sampling (Devroye, 1986) is used as the stochastic sampling. Then, ΔN laser rays are irradiated in the $(t+1)$-th scan.

4 EXPERIMENTS

We conducted the experiment for evaluating the peformance of the proposed method. The following sections explain details of the experimental settings and discuss the results.

4.1 Datasets

Since the hardware of an Active-scan LIDAR that can control the laser irradiation direction arbitrary and rapidly is still under development, we cannot use it for our experiments. Therefore, here we mimic the behavior of an Active-scan LIDAR by using dense point-clouds that are obtained by a higher density uniform scan LIDAR. For training, 400 point-clouds of pedestrians were collected (100 point-clouds for each pedestrian's orientation). Here, Velodyne LiDAR HDL-64E was used for obtaining point-clouds in a real-world environment, and these training data were used for generating the depth map and the local pedestrian likelihood map. On the other hand, for testing, we used the KITTI dataset (Geiger et al., 2012) and the Active-scan LIDAR was simulated using this dataset. Note that point-clouds in the KITTI dataset were also captured by Velodyne LiDAR HDL-64E. We carefully selected 600 scenes from the KITTI dataset so that a pedestrian without occlusion exists in the front (40°) of the vehicle. Here, all pedestrians existed closer than 30 m from the LIDAR.

4.2 Evaluation Methods

In this experiment, two methods were compared with the proposed method: the state-of-the-art previous method (Yamamoto et al., 2018), the comparative method, and the proposed method. The previous method (Yamamoto et al., 2018) does not consider pedestrian's orientation in Eq. (1) and does not use the effect of the term of $H(\boldsymbol{p} \mid \theta)$, that is, Eq. (9) is replaced with $H(\boldsymbol{p} \mid \theta) = 1$. The comparative method considers pedestrian's orientation θ which is a element of contributions but assumes $H(\boldsymbol{p} \mid \theta) = 1$. The proposed method uses all contributions presented in this paper. Other processes are exactly the same among all methods. Table 1 summarizes the conditions of each method.

Table 1: Evaluation methods.

	Prev.	Comp.	Prop.
Pedestrian's orientation		✓	✓
Depth-wise separation			✓

The following parameters were used in the experiments:

- Number of laser irradiations in the initial scan: $N_0 = 300$.
- Number of laser irradiations in each iteration (adaptive scan): $\Delta N = 100$.
- Number of iterations: 9 iterations.
- Total number of laser irradiations: $N_m = 1,200$.
- Vertical position of the initial scan: $h = 1.0$ m.
- Value of σ in Eq. (6): $\sigma = 0.1$ m.

These parameters were determined experimentally.

4.3 Evaluation Criteria

To evaluate the performance of each method, the following two evaluation criteria were employed:

The first criteria is the number of hit points N_{hit} that corresponds to the number of measured points from a target pedestrian. The higher this criterion is, the more the method can scan pedestrians adaptively.

The second criteria is the number of detected pedestrians N_{detect} that are composed of number of points above a threshold. The threshold is set to a value from 0 to 100 in a increment of 10. In order for the pedestrian detection method to appropriately classify each point-cloud into a pedestrian and a non-pedestrian, it is desirable that each point-cloud consists of a large number of points. Therefore, the higher this criterion is at a high threshold, the easier it is to detect pedestrians.

4.4 Results & Discussions

Figure 8 shows the results of all methods in each evaluation criterion.

As seen in the graphs, we can say that the comparative method outperforms the previous method in the criterion of detected pedestrians though the improvement of the number of hit points is minor. From this result, the use of orientation aware pedestrian likelihood map proposed in this paper can slightly improve the efficiency in the scan of pedestrians.

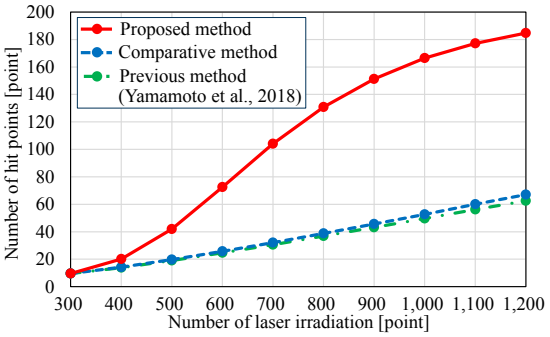

(a) Hit points.

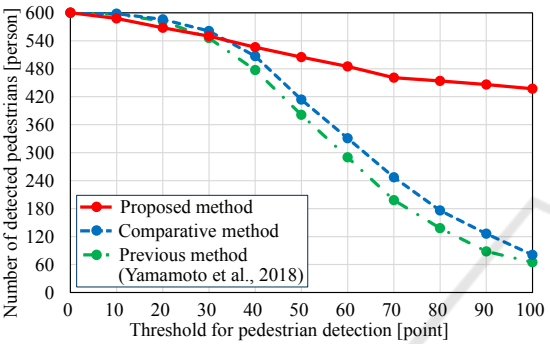

(b) Detected pedestrians.

Figure 8: Experimental results by two evaluation metrics.

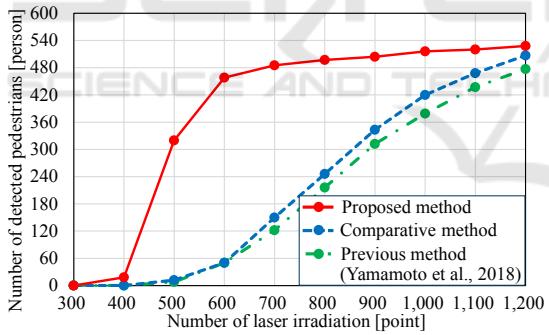

Figure 9: Transition of detected pedestrians using 40 points as the threshold.

On the other hand, the proposed method outperforms both the comparative and the previous methods in all evaluation criteria. Moreover, Figure 9 shows the transition of detected pedestrians when the threshold is set to 40 points. As seen in the graph, the proposed method is able to obtain point-clouds from pedestrians with less number of iteration than the other two methods.

Since the comparative and the previous methods use average integration of the local likelihood map by assuming that all measured points come from the same object, the resultant pedestrian likelihood map is blurred. On the other hand, the proposed method controls the integration weight of the local likelihood map according to the ratio of measured points coming from the same object judged by depth-wise object separation. Therefore, the proposed method could generate the pedestrian likelihood map intensively focusing on pedestrian regions, and the performance of the scan could be significantly improved. From these results, we confirmed the effectiveness of the combination of orientation aware pedestrian likelihood map and depth-wise object separation for improving the efficiency of the scan.

Figure 11 shows the results of the proposed method and the previous method applied to the scene shown in Fig. 10. From these results, we confirmed that the proposed method could efficiently control laser directions focusing on a pedestrian, and could achieve less laser irradiations than the previous method to dense obtain point-clouds from pedestrians.

5 CONCLUSIONS

In this paper, we proposed an efficient pedestrian scanning method based on the pedestrian likelihood map constructed by integrating an orientation aware local pedestrian likelihood map. Here, the local pedestrian likelihood map is integrated according to the weight related to the ratio of measured points that comes from the same object. In the proposed method, pedestrian scanning is formulated as a problem of stochastic sampling from the pedestrian likelihood map, where pedestrians can be scanned progressively by iterative scanning and map update.

To evaluate the performance of the proposed method, we conducted experiments by simulating the mechanism of an Active-scan LIDAR using the KITTI dataset. As a result, the proposed method outperformed comparative methods including the state-of-the-art method.

Future work will include an improvement of the local pedestrian likelihood map calculation, the development of a method to crop the pedestrians' point-clouds from point-clouds obtained by the proposed method, and experiments with larger datasets.

ACKNOWLEDGEMENTS

Parts of this research were supported by MEXT, Grant-in-Aid for Scientific Research.

Figure 10: Sample scene in the KITTI dataset (Geiger et al., 2012).

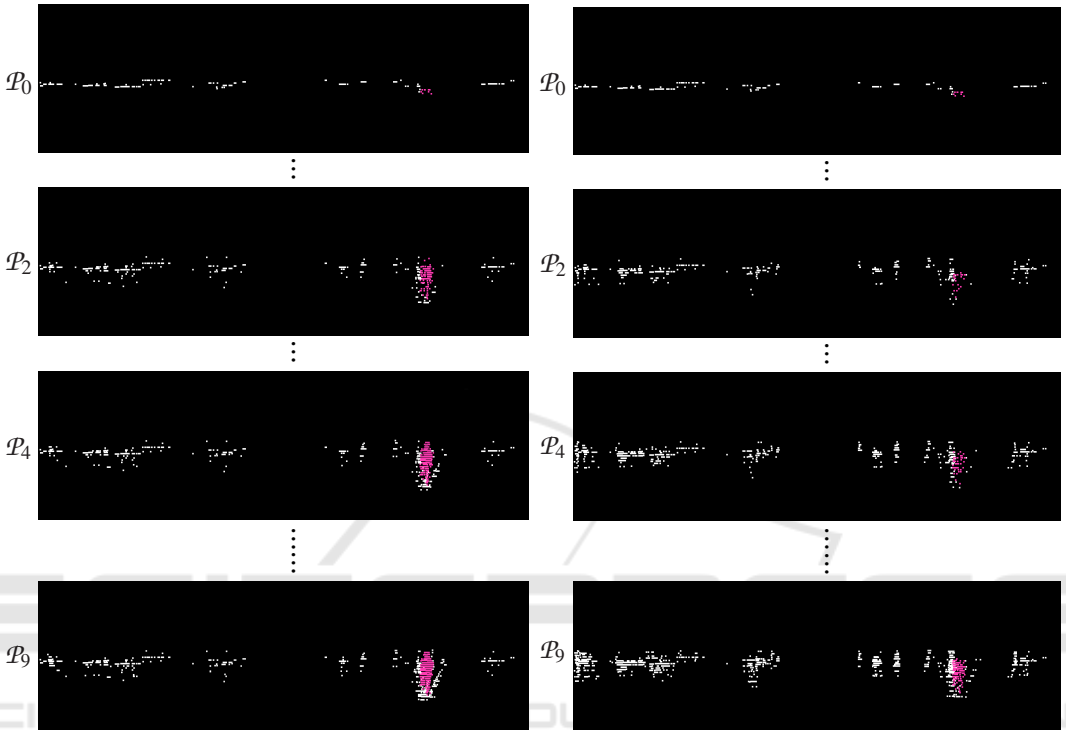

(a) Proposed method. (b) Previous method (Yamamoto et al., 2018).

Figure 11: Scanning results by the proposed method and the previous method (Yamamoto et al., 2018) applied to the scene in Fig. 10. Pink dots represent pedestrians while white dots represent other objects. $\mathcal{P}_t$ is a set of points obtained after the t-th scan.

REFERENCES

Behley, J., Steinhage, V., and Cremers, A. (Nov. 2013). Laser-based segment classification using a mixture of bag-of-words. In *Proc. 2013 IEEE/RSJ Int. Conf. on Intelligent Robots and Systems*, pages 4195–4200.

Devroye, L. (1986). *Non-uniform random variate generation*. Springer.

Geiger, A., Lenz, P., and Urtasun, R. (June 2012). Are we ready for autonoumous driving? The KITTI vision benchmark suite. In *Proc. 2012 IEEE Conf. on Computer Vision and Pattern Recognition*, pages 3354–3361.

Kidono, K., Miyasaka, T., Watanabe, A., Naito, T., and Miura, J. (June 2011). Pedestrian recognition using high-definition LIDAR. In *Proc. 2011 IEEE Intelligent Vehicles Symposium*, pages 405–410.

Maturana, D. and Scherer, S. (Sept. 2015). VoxNet: A 3D convolutional neural network for real-time object recognition. In *Proc. 2015 IEEE/RSJ Int. Conf. on Intelligent Robots and Systems*, pages 922–928.

Tatebe, Y., Deguchi, D., Kawanishi, Y., Ide, I., Murase, H., and Sakai, U. (Jan. 2018). Pedestrian detection from sparse point-cloud using 3DCNN. In *Proc. 2018 Int. Workshop on Advanced Image Technology*, pages 1–4.

Wang, H., Wang, B., Liu, B., Meng, X., and Yang, G. (Feb. 2017). Pedestrian recognition and tracking using 3D LIDAR for autonoumous vehicle. In *J. of Robotics and Autonoumous Systems*, volume 88, pages 71–78.

Yamamoto, T., Shinmura, F., Deguchi, D., Kawanishi, Y., Ide, I., and Murase, H. (Jan. 2018). Efficient pedestrian scanning by active scan LIDAR. In *Proc. 2018 Int. Workshop on Advanced Image Technology*, pages 1–4.

Zhou, Y. and Oncel, T. (June 2018). VoxelNet: End-to-end learning for point cloud based 3D object detection. In *Proc. 2018 IEEE Conf. on Computer Vision and Pattern Recognition*, pages 4490–4499.